Eleventh International Conference on Computational Fluid Dynamics (ICCFD11), Maui, Hawaii, USA, July 11-15, 2022

ICCFD11-2022-2201

Verification of nonequilibrium thermochemistry models for hypersonic CFD by first-principles simulation

E. Torres*, T. Gross*, E. Geistfeld* and T.E. Schwartzentruber*
Corresponding author: etorres@umn.edu

* Department of Aerospace Engineering and Mechanics, University of Minnesota
107 Akerman Hall, 110 Union St. SE Minneapolis, MN 55455-0153 USA

Abstract: In this paper, we present verification studies for the recently proposed Modified Marrone-Treanor [1] (MMT) thermochemical nonequilibrium model for computational fluid dynamics (CFD). We verify our CFD results using first-principles Direct Molecular Simulations (DMS) that rely only on potential energy surfaces (PESs) to determine all collision outcomes. Therefore, DMS is capable of naturally predicting vibrationally coupled excitation and dissociation of the gas under thermochemical nonequilibrium without any tuning parameters. The MMT model was developed using first-principles data for nitrogen and oxygen dissociation, but used legacy model parameters for Zel'dovich reactions. The present research performs first-principles simulations that now include all important interactions for dissociated air, including Zel'dovich reactions. The results are used to verify the accuracy of the MMT CFD model for a range of post-shock conditions, and suggest further modifications to improve the model. This research demonstrates how complex nonequilibrium chemistry induced by hypersonic flight can be incorporated into accurate and efficient models for large-scale CFD simulations.

Keywords: Thermochemical nonequilibrium, Hypersonic flow, Computational Fluid Dynamics, Modified Marrone-Treanor model, Direct Molecular Simulation.

1 Introduction

The DMS method [2] is a variant of direct simulation Monte Carlo [3] (DSMC) wherein collision outcomes are determined directly through classical trajectory calculations on multi-body potential energy surfaces (PES). Since it relies entirely on *ab initio* potentials to determine collision outcomes, DMS is capable of naturally predicting the vibrationally coupled excitation and dissociation of a gas mixture under thermochemical nonequilibrium conditions from first principles and without any tuning parameters. We use DMS results as benchmarks for the development of reduced-order nonequilibrium chemical-kinetics models for computational fluid dynamics (CFD). In our most recent work, we have demonstrated the capability of DMS to simulate chemically reacting air mixtures (including dissociation and exchange reactions) in isothermal heat baths [4], while relying exclusively on the most recent *ab initio* potentials from the computational chemists at the University of Minnesota [5]. In this paper, we build on these recent results by adapting and enhancing the thermodynamic and chemical-kinetic databases of US3D [6], the standard CFD code for hypersonic flow simulations at the University of Minnesota, to best reproduce the DMS predictions. This involves three main parts. First, as discussed in Sec. 2, we generate alternative fits to thermodynamic functions of air consistent with our *ab initio* potentials. Next, we adapt the vibrational relaxation models in US3D to best match the DMS behavior, as discussed in Sec. 3. Finally, in Sec. 4 we outline modifications and enhancements to an existing model for nonequilibrium dissociation in US3D in order to better match

DMS results. In particular, this involves generating new chemical-kinetic rate parameters for air species dissociation and Zel'dovich exchange reactions from quasi-classical trajectory (QCT) calculations on the same *ab initio* potentials employed by DMS. In this section we also compare CFD simulations against DMS solutions to determine how well the simplified CFD chemistry models can reproduce DMS behavior.

2 Thermodynamic properties for CFD to match DMS behavior

One of the most fundamental requirements for achieving good agreement between different numerical predictions of high-temperature reacting flows is to employ consistent thermodynamic properties (e.g. heat capacities, enthalpies and chemical equilibrium constants). In our particular case, we must ensure that the thermodynamic properties evaluated in the governing equations of our CFD model reproduce the microscopic behavior of DMS as closely as possible. In the space-homogeneous heat baths studied in this work, the thermodynamic properties are directly responsible for determining the final equilibrium state reached by the gas mixture. Typically, US3D relies on the NASA Lewis database to provide accurate thermodynamic data for flows relevant to high-temperature aerodynamics. The Lewis database was compiled at the NASA Lewis (now Glenn) Research center in the early 1990's and forms the basis of NASA's Chemical Equilibrium with Applications (CEA) program. Standard analytical expressions are used to compute the thermodynamic properties as functions of temperature (and pressure) from tabulated sets of 9-coefficient fit parameters covering the range between $T = 200\,\mathrm{K}$ and $20\,000\,\mathrm{K}$. For monatomic species, the thermodynamic properties include contributions of translational and electronic modes, whereas for polyatomic species, additional contributions from the molecules' rotational and vibrational modes are included.

Herein lies the major discrepancy between the thermodynamic properties predicted with the Lewis database and the behavior of the DMS model. The potential energy surfaces currently employed in our DMS calculations only allow for electronically adiabatic interactions between the ground electronic states of the colliding species. Thus, transitions to and from electronically excited states are not included in DMS and any molecules and atoms in the simulated mixture always remain in their respective ground states. For the five chemical species relevant in this work, the contributions of excited states to the thermodynamic properties become noticeable at different temperatures. Whereas for N_2 and NO electronic excitation does not play a major role below $5\,000\,\mathrm{K}$, the heat capacities of atomic nitrogen and oxygen begin to exhibit slight departures from the ground-state behavior above $2\,500\,\mathrm{K}$. Molecular oxygen possesses several excited states below its dissociation threshold, affecting its thermodynamic properties at even lower temperatures. In light of this restriction, in order to adapt the behavior of our CFD model to that of DMS, we must in a sense "downgrade" the thermodynamic properties used in US3D to exclude electronic energy. Clearly, by excluding electronic energy, CFD predictions at higher temperatures will be less accurate when being compared to experimental data. However, our main goal in this study is instead to achieve the closest agreement with DMS, which at present does not simulate electronic excitation.

We describe the manner in which we derive the thermodynamic properties for all mixture components based entirely on characteristics of the potential energy surfaces in App. B of Ref. [7], with oxygen as an example. In short, we rely exclusively on characteristics of the diatomic potential energy curves for N_2, O_2 and NO derived from the Minnesota PESs to compute the rovibrational energy levels and associated internal partition functions. With all thermodynamic properties being computed from the partition functions alone, we perform a fit to the 9-coefficient analytical form over the same temperature range of the Lewis database. These modified fit parameters then allow US3D to automatically reproduce ground-state-only properties that are the most consistent with the DMS behavior.

The magnitude of the differences between both sets of properties is illustrated by the following plots. First, species enthalpies per unit mole are compared in Fig. 1. The three diatomic species (N_2: red, O_2: blue and NO: green) are shown in Fig. 1(a), while the two monatomic ones (N_2 in light orange, O_2 in light blue) are shown in Fig. 1(b). We have labeled the properties based on the UMN PES-derived partition functions as "PES" (solid lines) and the ones from the Lewis database as "Lewis" (dotted lines). As can be seen, contributions of electronic excited states of all five species tend to increase their respective enthalpies at higher temperatures.

In Fig. 2, we compare the equilibrium constants obtained from the UMN PES-derived partition functions (dotted lines) with those from the Lewis fits (solid lines). First, in Fig. 2(a) we plot the equilibrium constants

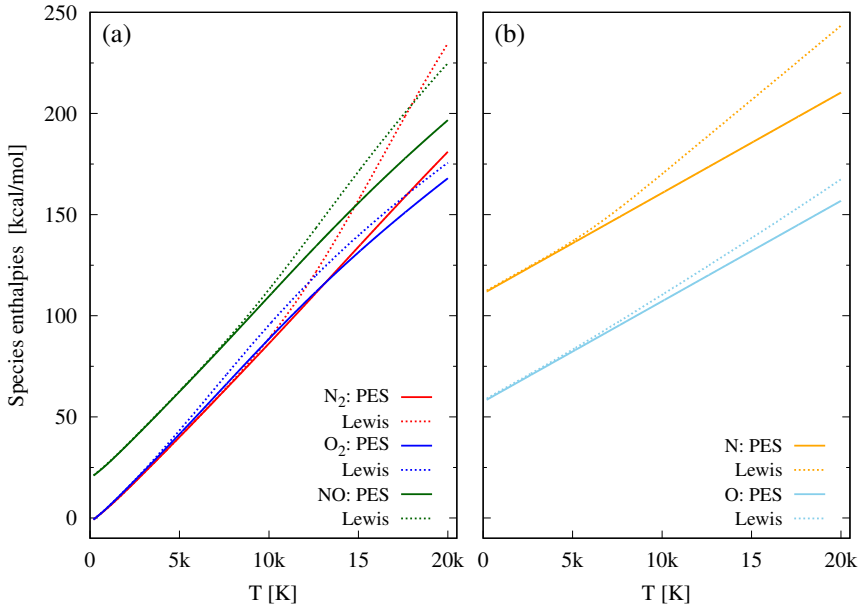

Figure 1: Species enthalpies per unit mole for 5-species air, derived from UMN diatomic PES energy levels (continuous) vs. CEA Lewis fits (dotted)

in terms partial pressure ratios for the molecular species and their respective atomic constituents: $K_p^{\mathrm{N_2}\rightleftharpoons\mathrm{N}} = p_{\mathrm{N}}^2/p_{\mathrm{N_2}}$ (red), $K_p^{\mathrm{O_2}\rightleftharpoons\mathrm{O}} = p_{\mathrm{O}}^2/p_{\mathrm{O_2}}$ (blue) and $K_p^{\mathrm{NO}\rightleftharpoons\mathrm{N+O}} = p_{\mathrm{N}}\,p_{\mathrm{O}}/p_{\mathrm{NO}}$ (green). Then, in Fig. 2(b) we report the two equilibrium constants between the reactants and products of the two Zel'dovich exchange reactions: $K_p^{\mathrm{NO+O}\rightleftharpoons\mathrm{O_2+N}} = p_{\mathrm{O_2}}\,p_{\mathrm{N}}/p_{\mathrm{NO}}\,p_{\mathrm{O}}$ (light blue) and $K_p^{\mathrm{N_2+O}\rightleftharpoons\mathrm{NO+N}} = p_{\mathrm{NO}}\,p_{\mathrm{N}}/p_{\mathrm{N_2}}\,p_{\mathrm{O}}$ (orange). Minor differences between both sets of equilibrium constants can be observed. For the dissociation reactions, the deviations seem to be more prominent at higher temperatures. For the exchange reactions, they seem to be present over the entire temperature range. However, the aggregate effect of all these differences can best be quantified with the help of an example containing all five chemical species.

We examine the effect of the modified thermodynamic properties with the help of two simple test cases. With US3D, we simulate the evolution of a gas mixture initially out of thermo-chemical equilibrium in a space-homogeneous (0D), adiabatic reactor. The initial conditions are meant to approximate air being rapidly heated after traversing a strong shock wave, such as the one forming ahead a of hypersonic flight vehicle, or atmospheric entry capsule. The gas density in the reactor remains constant at $\rho = 0.01\,\mathrm{kg}\cdot\mathrm{m}^{-3}$, with the initial mole fractions set to $x_{\mathrm{N_2}} = 0.79$ and $x_{\mathrm{O2}} = 0.21$. The initial trans-rotational temperature is first set to $T_{\mathrm{tr}} = 10\,000\,\mathrm{K}$, while the vibrational (-electronic) temperature of the diatomic species is initially set to $T_{\mathrm{v}} = 300\,\mathrm{K}$. A second set of simulations is run, where the trans-rotational temperature is initialized at $T_{\mathrm{tr}} = 20\,000\,\mathrm{K}$. We perform each simulation twice, first relying on the standard Lewis fits (which account for electronic excitation) to compute all thermodynamic properties and then switch over to our own custom fits (which exclude electronic energy contributions). We restrict the set of chemical species to "five-species air", i.e. $\mathrm{N_2}$, $\mathrm{O_2}$, NO, N and O. Thus, no ionized species, nor free electrons are allowed to form in either case. The chemical-kinetic model, along with vibrational relaxation times are taken from Park [8]. Note that for this comparison the precise choice of vibrational relaxation model and reaction rate data is of secondary importance, since we are only concerned with the final equilibrium state.

In Fig. 3, we compare the results of the first set of simulations. The time evolution of T_{tr} (black) and T_{v} (gray) are plotted in the left sub-figure, with the corresponding evolution of the mixture mole fractions on the right. Dotted lines labeled as "Lewis" represent the results when using the Lewis fits, while solid lines labeled as "PES" are the corresponding ones resulting from using our custom fits. As can be seen, at this set of conditions, the departure between the "Lewis" and "PES" curves is barely noticeable. For easier comparison, all numerical values are listed in Table 1. For the first test case, columns 3 and 4 list the equilibrium temperatures and mixture compositions attained by the "Lewis" and "PES" fits respectively.

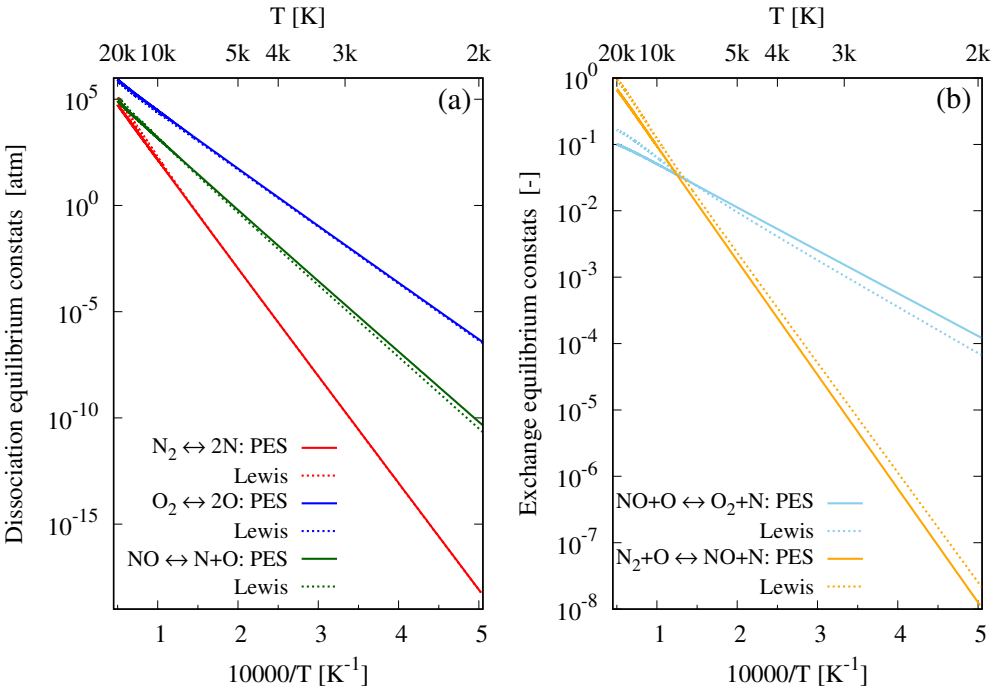

Figure 2: Equilibrium constants for 5-species air, derived from UMN diatomic PES energy levels (continuous) vs. CEA Lewis fits (dotted)

For the temperature, a relative discrepancy of less than 1% is observed. With both sets of thermodynamic properties, at first glance, the equilibrium composition looks almost identical. Practically all of the initial O_2 has disappeared and only a tiny amount of atomic nitrogen has formed. Relative discrepancies between the equilibrium mole fractions for N_2 and O predicted by the Lewis fits and our own do not exceed 1%. The discrepancy for NO lies at about 7% and is most severe for the two trace species (12-22%). However, for this case the overall equilibrium mixture composition is not altered significantly by ignoring electronic energy contributions.

In Fig. 4, we now compare the second set of simulations. All data are labeled following the convention introduced in Fig. 3. Since this is a higher-enthalpy condition, the gas equilibrates at a higher final temperature. It also exhibits a stronger degree of dissociation compared to Case 1, as can be seen in columns 7 and 8 of Table 1. Indeed, the only molecular species remaining in any significant amount is N_2. The remainder of the mixture consists almost entirely nitrogen and oxygen atoms.

Though subtle to observe, both cases exhibit common behavior. When using the Lewis fits, the final equilibrium temperature is slightly lower and the gas is "less dissociated" (i.e. larger equilibrium mole fractions of diatomic species) than with the PES fits. This is consistent with the fact that the thermodynamic properties of the Lewis fits account for additional electronic energy. Thus, part of the initial trans-rotational energy is re-distributed into the electronic mode and tends to further lower the final equilibrium temperature. Since dissociation reactions are endothermic, re-distributing a fraction of the initial trans-rotational into electronic modes also removes some energy needed to dissociate molecular species. By contrast, when using the PES fits, the additional "energy sink" of electronic modes is missing. Thus, more of the initial energy is available to raise the gas' final temperature and to promote a greater degree of dissociation. The differences between both sets of thermodynamic properties on the final equilibrium conditions for both cases studied are still relatively minor. This is because, all things considered, the final equilibrium temperatures remain fairly "low". Even at the higher-enthalpy condition, the final temperature does not exceed 6 000 K. Since departures between the Lewis and PES enthalpies remain fairly small below this temperature (recall Fig. 1), this is not too surprising. In later sections of this work, we will study heat baths at higher temperatures. There, the departures between both sets of thermodynamic properties would be more significant. However,

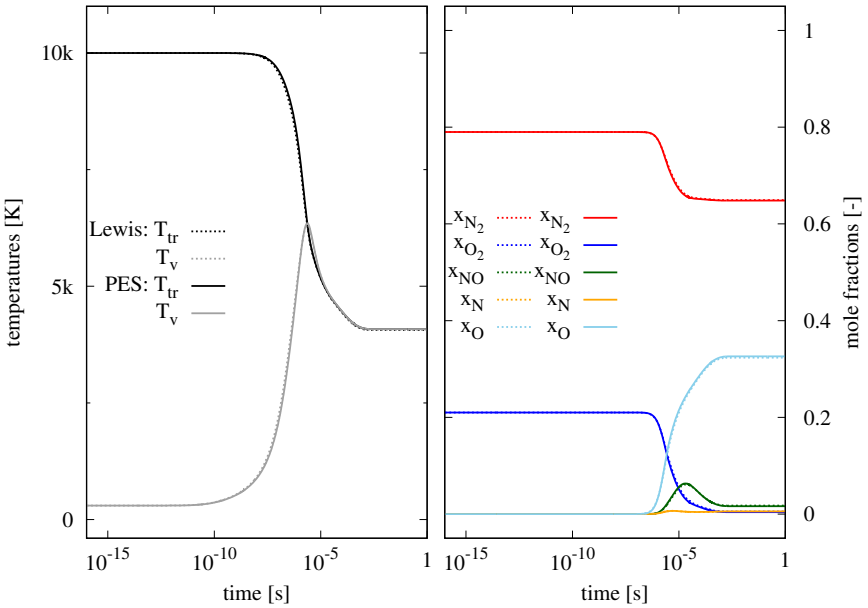

Figure 3: Effect of thermodynamic property fits on equilibrium state in adiabatic reactor. Case 1: initial $T_{\mathrm{tr}} = 10\,000\,\mathrm{K}$

Table 1: Comparison of thermodynamic behavior of Lewis fits vs. PES fits for 5-species air in adiabatic reactor.

	Case 1 initial	eq. Lewis	eq. PES	diff. (%)	Case 2 initial	eq. Lewis	eq. PES	diff. (%)
T_{tr} [K]	10 000	4 065.8	4 082.1	0.4	20 000	5 805.1	5 809.7	0.1
T_{v} [K]	300				300			
$x_{\mathrm{N_2}}$	0.7900	0.6492	0.6482	−0.2	0.7900	0.4542	0.4490	−1.2
$x_{\mathrm{O_2}}$	0.2100	0.0052	0.0040	−22.4	0.2100	0.0001	0.0001	−19.9
x_{NO}	0	0.0175	0.0163	−7.2	0	0.0039	0.0037	−4.8
x_{N}	0	0.0048	0.0054	12.3	0	0.2396	0.2460	2.7
x_{O}	0	0.3232	0.3261	0.9	0	0.3022	0.3012	−0.3

since those calculations involve direct comparisons with DMS data only, the PES-derived thermodynamic properties will be used with US3D.

3 Characteristic vibrational relaxation times derived from DMS

In this section, we discuss how we have modified the built-in vibrational relaxation behavior of US3D to one that more closely mimics that of DMS. By default, US3D simulates the relaxation of trans-rotational and vibrational modes toward a common temperature by means of a source term in the vibrational energy equation. When the relaxation term is considered in a space-homogeneous isolated system without the influence of chemical reactions, this equation reads:

$$\frac{\mathrm{d}E_v}{\mathrm{d}t} = \sum_{s\in\mathcal{D}} \rho_s \frac{e^{\star}_{v,s}(T_{\mathrm{tr}}) - e_{v,s}(T_{\mathrm{v}})}{\langle \tau^v_s \rangle}, \tag{1}$$

where the left hand side represents the time rate of change of mixture vibrational energy density. The source term on the right hand side consists of a partial-density-weighted sum over all vibrationally relaxing diatomic species $\mathcal{D} = \{\mathrm{N_2}, \mathrm{O_2}, \mathrm{NO}\}$. Each species' contribution is modeled as a Landau-Teller relaxation term,

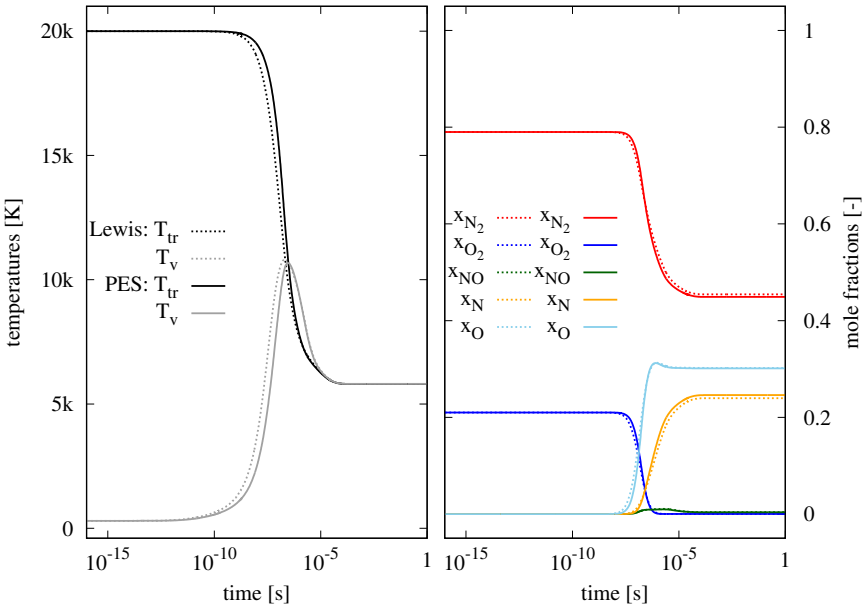

Figure 4: Effect of thermodynamic property fits on equilibrium state in adiabatic reactor. Case 2: initial $T_{\mathrm{tr}} = 20\,000\,\mathrm{K}$

where the numerator represents the departure of the species' specific vibrational energy at the instantaneous vibrational temperature $e_{v,s}(T_{\mathrm{v}})$ from the corresponding equilibrium value at the local gas trans-rotational temperature $e^{\star}_{v,s}(T_{\mathrm{tr}})$. The term in the denominator represents the effective characteristic relaxation time of each relaxing species. It is itself computed as a sum over all collision partners $\mathcal{S} = \{\mathrm{N}_2, \mathrm{O}_2, \mathrm{NO}, \mathrm{N}, \mathrm{O}\}$, weighted by their respective mole fractions x_r:

$$\langle \tau_s^v \rangle = \left(\sum_{r \in \mathcal{S}} \frac{x_r}{\tau_{sr}^v} \right)^{-1} \tag{2}$$

The pair-wise relaxation times τ_{sr}^v are ultimately the quantities that govern the relaxation rate of each species and must be provided from an external source. US3D computes them based on the Millikan-White (M&W) correlation [9] as a function of gas temperature and pressure. On top of this, the high-temperature correction as described by Park [8] is applied to prevent the value of the different $\langle \tau_s^v \rangle$ to become nonphysically small at higher temperatures. By default, US3D relies on parameters for the M&W correlation and high-temperature correction for air species listed in Ref. [8].

In recent work [4], we used DMS to obtain independent estimates of vibrational relaxation times from purely molecular-scale calculations. These calculations have revealed that for many species the DMS predictions deviate from the standard M&W+Park correlations, especially at high temperatures. For a few examples, consult Figs. 2-5 in the cited reference. The magnitudes of these deviations are also illustrated in Fig. 5, where we show Landau-Teller plots for a few of the most relevant air species. Predictions for $\tau_{sr}^v \cdot p$ with the Millikan-White correlation are shown as red lines, the ones including Park's high-temperature correction as black lines and the raw relaxation time estimates from DMS as blue symbols. As discussed in Ref. [4], the DMS data were collected in isothermal heat bath calculations (without chemical reactions) ranging from temperatures as high as 100 000 K to as low as 3 000 K in some instances. It should be noted that DMS calculations to extract vibrational relaxation times at lower temperatures become too time consuming to be practically feasible. Thus, the low-temperature limiting behavior of the DMS data was extrapolated based on observed trends. While species pairings, such as $\mathrm{N}_2 - \mathrm{N}_2$, $\mathrm{O}_2 - \mathrm{O}_2$ and $\mathrm{O}_2 - \mathrm{N}_2$ do asymptotically approach the low-temperature Millikan-White behavior, others such as $\mathrm{N}_2 - \mathrm{N}$, $\mathrm{N}_2 - \mathrm{O}_2$ and in particular $\mathrm{O}_2 - \mathrm{O}$ do not seem to follow the same trends.

Since our goal is to provide US3D with new vibrational relaxation times that best match those of our

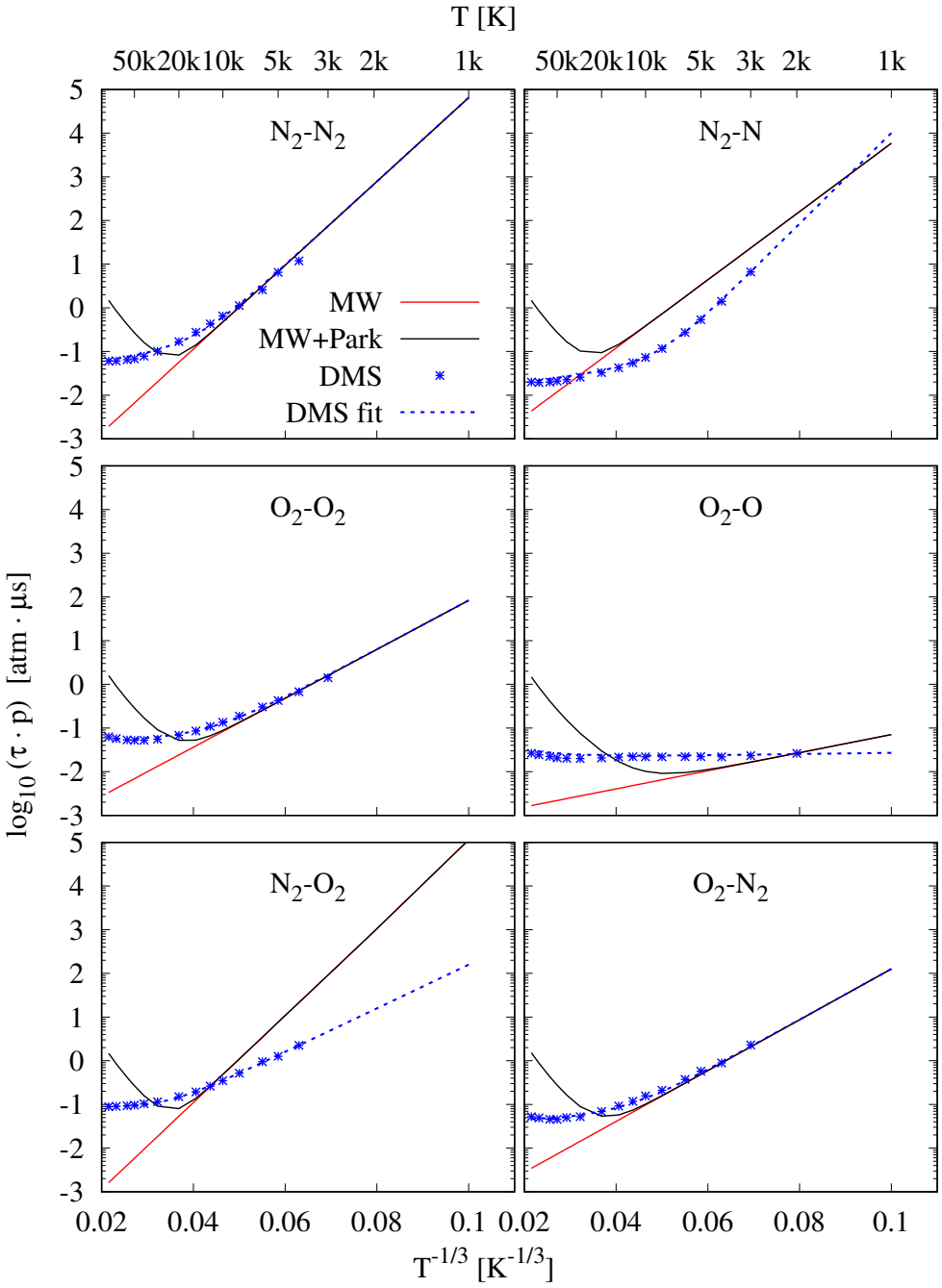

Figure 5: Landau-Teller plots for vibrational relaxation times of selected species pairs. Millikan-White correlation (red), M&W plus Park high-temperature correction (black), raw DMS estimates (blue symbols), fit to DMS (dashed blue)

Table 2: Choice of fitting function used for estimating τ_{sr}

	N_2	O_2	NO	N	O
N_2	DMS fit	DMS fit	∞	DMS fit	DMS fit
O_2	DMS fit	DMS fit	∞	DMS fit	DMS fit
NO	∞	∞	MW+Park	MW+Park	MW+Park

DMS calculations, the need for a new manner to fit those DMS data arose. It was found that all data could be represented with good accuracy by the functional form:

$$\tau_{sr}^{v} \cdot p = \exp\left(m_{sr}^{\text{low}}\, T^{-1/3} + n_{sr}^{\text{low}}\right) + \exp\left(m_{sr}^{\text{high}}\, T^{-1/3} + n_{sr}^{\text{high}}\right) \tag{3}$$

The form of Eq. (3) can be thought of as a "two-slope" Millikan-White expression, with one exponential term responsible for the low-temperature limiting behavior and the other one taking care of the high-temperature limit. The results of fitting the DMS data to this functional form are shown in Fig. 5 as dashed blue lines. Similar fits were produced for some of the remaining species pairs in Air5 (e.g. $O_2 - N$), but are not shown here. We should note that in many instances, especially those involving NO-vibrational relaxation the DMS data are incomplete. This problem is mentioned in Ref. [4] and has further implications for the chemistry study in Sec. 4. In short, the set of potential energy surfaces needed to carry out trajectory calculations for all species pairings in air is still incomplete. Therefore, an exhaustive set of fits for all pairings could not be generated. We summarize the current state of affairs in Table 2. For all entries listed as "DMS fit", we had DMS data available to fit to Eq. (3). For entries marked as "∞" no suitable potential energy surfaces exist at the moment and these interactions are effectively ignored in our DMS calculations. Thus, in our current DMS implementation encounters between these collision pairs do not promote vibrational relaxation of either species. To mimic this behavior in US3D, we impose fit parameters for Eq. (3) that generate very large vibrational relaxation times for these pairings, essentially approaching infinity. A few of the remaining interactions (third row) do occur in DMS, but the Landau-Teller plots from DMS relaxation data have not been constructed yet. For the time being, we continue to use the existing M&W+Park correlations for these interactions.

An exhaustive verification of integrating all new DMS fits into US3D is beyond the scope of this paper, but a small sample is given in what follows. We use US3D to carry out vibrational relaxation studies in space-homogeneous, isothermal reservoirs in the absence of chemical reactions at constant heat bath trans-rotational temperatures $T_{\text{tr}} = 4\,000\,\text{K}$ and $T_{\text{tr}} = 20\,000\,\text{K}$. Initially, a vibrational temperature of $T_{\text{v}} = 300\,\text{K}$ is imposed for the gas. We then simulate its relaxation toward thermal equilibrium. In Fig. 6, we show the results of these calculations for reservoirs containing pure molecular nitrogen (upper row) and mixtures containing an $N_2 - N$ mixture with a mole fraction ratio of 50%/50% (lower row). This problem is exactly described by Eq. 1, where the sum extends only over species $s = N_2$ and the vibrational relaxation time is either $\langle \tau_{N_2}^{v} \rangle = \tau_{N_2\,-\,N_2}^{v}$ for the pure N_2-gas, or $\langle \tau_{N_2}^{v} \rangle = \left(0.5/\tau_{N_2\,-\,N_2}^{v} + 0.5/\tau_{N_2\,-\,N}^{v}\right)^{-1}$ for the mixture. Depending on the reservoir temperature, vibrational relaxation of N_2 occurs over vastly different time scales. As would be expected, at $T_{\text{tr}} = 4\,000\,\text{K}$ (left column), it takes much longer than at $20\,000\,\text{K}$ (right column). Three sets of curves are plotted in each case: First, the relaxation curve predicted by US3D according to the original MW+Park correlation in red. Next, the new DMS fit predicted by US3D as black lines and finally an analytical solution to the same problem represented by black squares. As can be seen, for pure N_2 relaxation at $4\,000\,\text{K}$, both the original M&W+Park correlation and the DMS fit give the same answer. This is to be expected, since the DMS fit was extrapolated to follow the M&W curve at low temperatures. By contrast, at $20\,000\,\text{K}$, the DMS fit predicts a slightly slower relaxation behavior than the M&W+Park correlation, which is also in line with the corresponding Landau-Teller plots. When atomic nitrogen is added to the mix, the average vibrational relaxation times predicted by the DMS fits become noticeably shorter compared to the M&W+Park correlation (lower row). Both at $4\,000\,\text{K}$ and at $20\,000\,\text{K}$, the DMS fits (black curves) lead the M&W+Park correlation (red curves) by a significant amount. Again, this is consistent with the deviations between the DMS data and the correlation observed in the Landau-Teller plot of $N_2 - N$ shown in Fig. 5.

An equivalent verification study was carried out for oxygen and the results are shown in Fig. 7. The same two reservoir temperatures were simulated, but now using either pure O_2 (upper row), or an $O_2 - O$ mixture

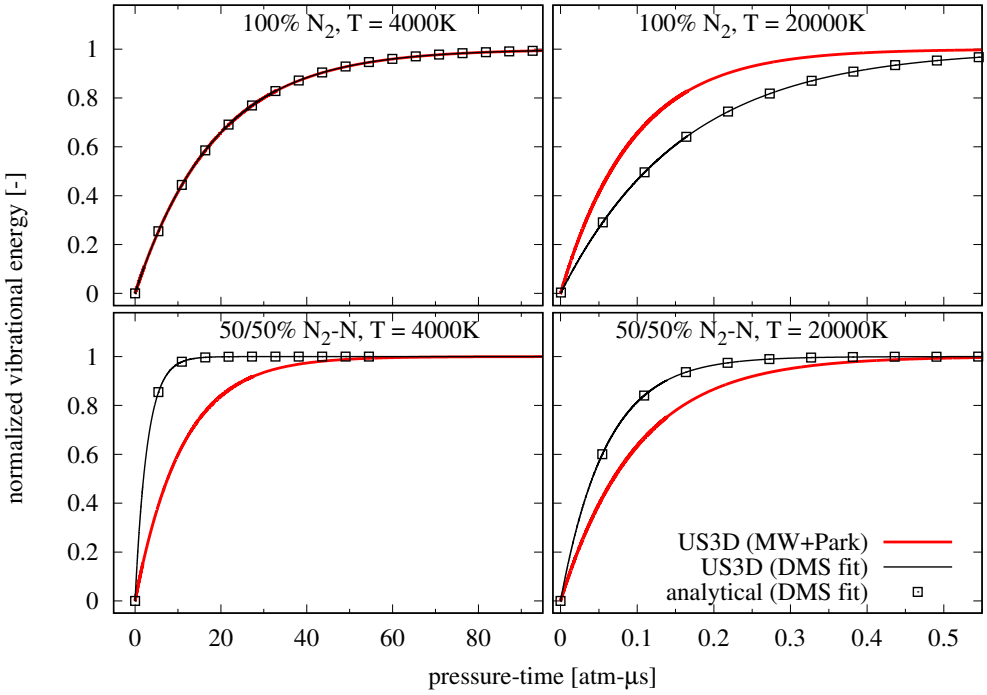

Figure 6: Vibrational relaxation of nitrogen in isothermal heat bath

with a mole fraction ratio of 50%/50% (lower row). Now, the relaxation curves predicted by US3D according to the original MW+Park correlation are shown in blue, the new DMS fit predicted by US3D as black lines and the analytical solution to the same problem is again represented by black squares. When compared to the nitrogen relaxation of Fig. 6, we see that the departure of the DMS fits from the M&W+Park predictions is much less severe for oxygen. And, especially at 4 000 K vibrational relaxation in oxygen occurs much faster than in nitrogen.

Figures 6 and 7 serve to illustrate differences in vibrational relaxation behavior between the DMS fits and the original M&W+Park correlations. In some instances the differences are quite noticeable, in others the two predictions closely agree. With the DMS fits incorporated into US3D, we move on to the main part of this work. The following section discusses improvements to a nonequilibrium chemistry model for air, which will allow US3D to best reproduce the DMS behavior.

4 Updates to MMT chemistry model for CFD

The MMT model was originally implemented by Chaudhry et al. [1] into US3D. The MMT kinetic rate parameters for nonequilibrium N_2- and O_2-dissociation were generated from quasi-classical trajectory (QCT) calculations [10, 11] on the Minnesota *ab initio* potentials. The model has since then been employed in several vehicle-scale simulations of hypersonic flows [12, 13, 14].

We should recall that what we refer to as "the MMT model" consists of several parts. First, the collection of Arrhenius rate parameters for nitrogen and oxygen dissociation derived from extensive QCT calculations. Second, the expressions and fit parameters needed to compute the nonequilibrium dissociation factors $Z(T_{\mathrm{tr}}, T_{\mathrm{v}})$, vibrational energy removed per dissociation reaction $\langle \varepsilon_{\mathrm{vib}} \rangle_d$, in addition to so-called non-Boltzmann correction factors α_k^{NB} and $\alpha_\varepsilon^{\mathrm{NB}}$. Wheras the Arrhenius parameters by themselves allow us to evaluate the *thermal* dissociation rate coefficients at equilibrium temperature T, it is only once the additional parameters are included that the MMT model can be used to accurately predict nonequilibrium dissociation in a post-shock environment. It should further be mentioned that the original version of the MMT model included QCT-derived Arrhenius parameters only for a subset of all Air-5 reactions. At the time many potential energy surfaces necessary for generating an exhaustive set of QCT-derived rate data

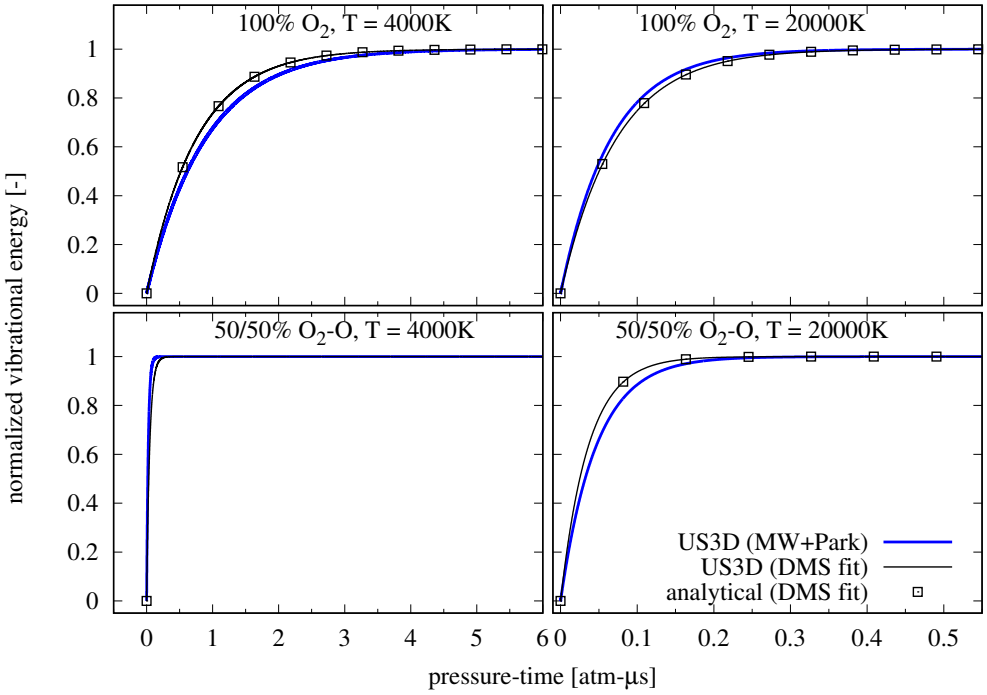

Figure 7: Vibrational relaxation of oxygen in isothermal heat bath

were unavailable. This led to the use of alternative sources to fill in the gaps. The provenance of rate data used in the first version of the MMT model is summarized in Table 3. As can be seen, dedicated QCT-derived parameters were only available for the main N_2- and O_2-dissociation reactions, i.e. 1,2,4,6,7 and 10. Some of these parameters were "re-used" to estimate N_2- and O_2-dissociation rates with the collision partners NO, O and N. Further reactions of major importance include the two Zel'dovich exchange and NO-dissociation reactions. As can be seen from Table 3, these reactions were still computed using Park's 1993 [8] rates. In what follows, we will refer to this version as MMT (2020).

Recent work [4] has yielded new QCT-derived rate parameters for the Zel'dovich exchange reactions, $O_2 + N \rightleftharpoons NO + O$ and $N_2 + O \rightleftharpoons NO + N$, which now replace the older Park 1993 data. The current reaction set with all recent modifications is summarized in Table 4. As can be seen, we have also generated new QCT-derived rate data for some of the remaining dissociation reactions (reactions 7-10). However, a full set of rate data for Air-5 cannot be generated from QCT due to certain missing PESs. In particular, this affects reactions 7,9 and 10, as well as the entirely missing reactions involving $N_2 + NO$ and $O_2 + NO$ collision pairs. Since our current goal is to make the MMT model as consistent as possible for comparisons with DMS, we have opted for not including these reactions at all. This means that this updated reaction set removes all of the "re-used" dissociation rates from Table 3. In what follows, we refer to the updated set as the MMT (2022) model.

We now examine the effect of our recent modifications to the MMT rate data with the help of a simple test case. We use US3D to simulate the coupled vibrational relaxation and nonequilibrium chemistry of an air-5 mixture in a space-homogeneous, constant-temperature, constant-volume reactor. The heat bath's trans-rotational temperature is kept at $T_{\mathrm{tr}} = 10\,000\,\mathrm{K}$. The gas has an initial vibrational temperature of 300 K, an initial pressure of 1.36 atm, with initial mole fractions $x_{N_2} = 0.8$ and $x_{O_2} = 0.2$. We compare our results to a DMS calculation starting from equivalent initial conditions.

In the first US3D run, we employ the Park $\sqrt{T\,T_v}$ chemistry model and associated rate data for Air-5 from 1993 [8]. The time evolution of the mixture composition is shown in the left half of Fig. 8 and covers the first 7 μs of the process. The US3D mixture composition (dotted lines) is compared to equivalent data extracted from DMS (solid lines). The right half of Fig. 8 shows the corresponding time history of vibrational

[1]Based on recent, partially published [4] QCT rate data

Table 3: Reaction types included in original MMT model (2020 version) for air-5 [1].

	Type	Reaction	Model/Rates used	comment
1	diss	$N_2 + N_2 \rightleftharpoons N + N + N_2$	MMT 2020	QCT-derived [10]
2	diss	$N_2 + O_2 \rightleftharpoons N + N + O_2$	MMT 2020	QCT-derived [11]
3	diss	$N_2 + NO \rightleftharpoons N + N + NO$	MMT 2020	same as (1)
4	diss	$N_2 + N \rightleftharpoons N + N + N$	MMT 2020	QCT-derived [10]
5	diss	$N_2 + O \rightleftharpoons N + N + O$	MMT 2020	same as (4)
6	diss	$O_2 + N_2 \rightleftharpoons O + O + N_2$	MMT 2020	QCT-derived [11]
7	diss	$O_2 + O_2 \rightleftharpoons O + O + O_2$	MMT 2020	QCT-derived [11]
8	diss	$O_2 + NO \rightleftharpoons O + O + NO$	MMT 2020	same as (10)
9	diss	$O_2 + N \rightleftharpoons O + O + N$	MMT 2020	same as (10)
10	diss	$O_2 + O \rightleftharpoons O + O + O$	MMT 2020	QCT-derived [11]
11	diss	$NO + M \rightleftharpoons N + O + M$	Park 1993	
12	exch	$N_2 + O \rightleftharpoons NO + N$	Park 1993	
13	exch	$NO + O \rightleftharpoons O_2 + N$	Park 1993	

Table 4: Reaction types included in updated MMT model (2022 version) for direct comparison with DMS.

	Type	Reaction	Model/Rates used	comment
1	diss	$N_2 + N_2 \rightleftharpoons N + N + N_2$	MMT 2020	QCT-derived [10]
2	diss	$N_2 + O_2 \rightleftharpoons N + N + O_2$	MMT 2020	QCT-derived [11]
3	diss	$N_2 + N \rightleftharpoons N + N + N$	MMT 2020	QCT-derived [10]
4	diss	$O_2 + O_2 \rightleftharpoons O + O + O_2$	MMT 2020	QCT-derived [11]
5	diss	$O_2 + N_2 \rightleftharpoons O + O + N_2$	MMT 2020	QCT-derived [11]
6	diss	$O_2 + O \rightleftharpoons O + O + O$	MMT 2020	QCT-derived [11]
7	diss	$N_2 + O \rightleftharpoons N + N + O$	MMT 2022	QCT-derived [1] (partial PESs)
8	diss	$O_2 + N \rightleftharpoons O + O + N$	MMT 2022	QCT-derived [1]
9	diss	$NO + N \rightleftharpoons N + O + N$	MMT 2022	QCT-derived [1] (partial PESs)
10	diss	$NO + O \rightleftharpoons N + O + O$	MMT 2022	QCT-derived [1] (partial PESs)
11	exch	$N_2 + O \rightleftharpoons NO + N$	MMT 2022	QCT-derived [1]
12	exch	$NO + O \rightleftharpoons O_2 + N$	MMT 2022	QCT-derived [1]

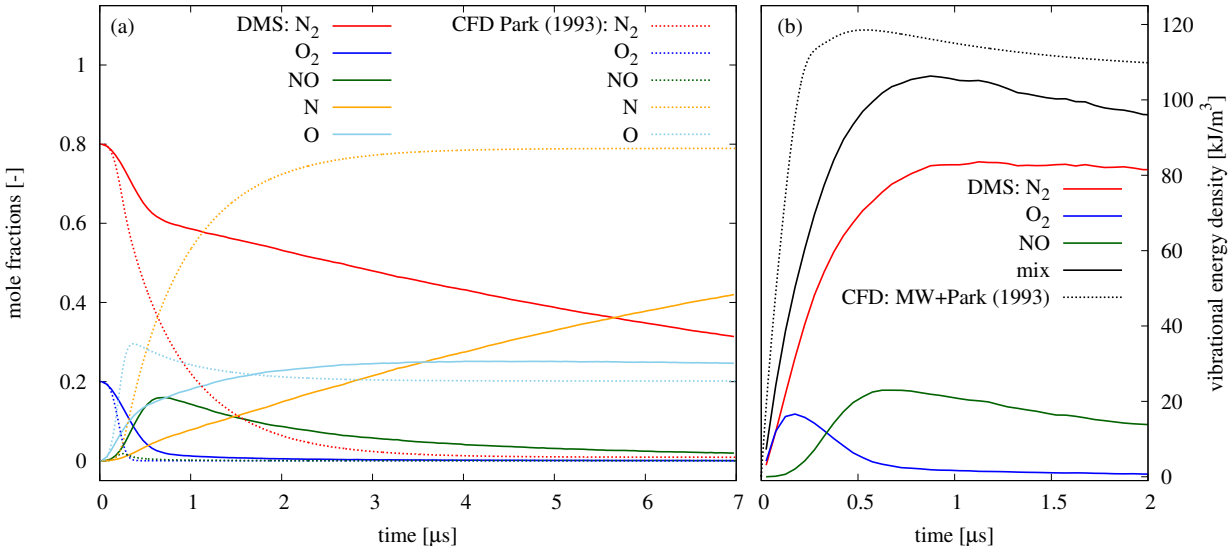

Figure 8: Isothermal heat bath at $T = 10\,000\,\mathrm{K}$. Left: Species mole fractions from DMS (solid lines) vs. US3D with Park $\sqrt{T\,T_v}$ model (dotted lines). Right: vibrational temperatures from DMS (solid lines) vs. US3D with M&W + Park HT correction (dotted lines) for τ_v.

energies for the first $2\,\mu$s. Here, US3D (dotted black line) employs the Millikan & White correlation, plus Park's high-temperature correction for evaluating the relaxation times. The necessary fit parameters are again those listed by Park [8]. This calculation is meant to establish a baseline for our comparison, since the Park model is still widely used in hypersonic CFD calculations. Clearly, there are significant differences in how the mixture composition evolves according to the Park rates as compared to DMS. Both O_2 and N_2 are depleted at a much faster rate in the US3D solution, when compared to DMS. The CFD solution seems to evolve at a rate roughly one order of magnitude faster than DMS. In fact, past the first $5\,\mu$s it has effectively reached its final equilibrium state. The other major difference to observe is that the CFD solution predicts negligible amounts of NO being produced, whereas in the DMS profiles its mole fraction peaks at just under 0.18.

A direct comparison of vibrational temperature profiles is more difficult. The governing equations in US3D include one balance equation to track the average vibrational energy density of the gas mixture $E_v = \rho_{\mathrm{N_2}} e_{v,\mathrm{N_2}} + \rho_{\mathrm{O_2}} e_{v,\mathrm{O_2}} + \rho_{\mathrm{NO}} e_{v,\mathrm{NO}}$. An underlying assumption in this description is that the vibrational modes of all three diatomic species are always equilibrated at the common vibrational temperature T_v. Thus, only a single vibrational temperature can be extracted from the CFD solution. By contrast, DMS tracks the vibrational energies of all simulated diatomic particles and it is possible to extract separate vibrational temperatures for each diatomic species. We reported such temperatures for this test case in our recent work [4]. The red, blue and green curves in Fig. 6(b) of the cited reference are obtained for the vibrational temperatures of N_2, O_2 and NO respectively. Unlike DMS, the CFD solution cannot capture the departure between species vibrational temperatures and, most notably, cannot predict that NO is formed "vibrationally hot", approximately at the heat bath trans-rotational temperature. For an easier comparison we examine the mixture vibrational energy densities E_v instead. The CFD profile (dotted black line) appears in Fig. 8(b). It can be compared to the corresponding DMS curve (solid black line) for the mixture vibrational energy, along with the individual contributions of all three diatomic species. The rise in average vibrational energy density predicted by US3D is faster than with DMS. It reaches a higher peak and then decays at a slower rate than the DMS curve.

In the second US3D run, we swap out the Park model in favor of the original version of the MMT model (MMT 2020). We continue to use the Millikan & White correlation, plus Park's high-temperature correction for evaluating the vibrational relaxation times. The comparison is shown in Fig. 9, where all data plotted following the same conventions as before. As can be seen in Fig. 9(a), during the first $0.5\,\mu$s the US3D solution using the MMT 2020 rates is in closer agreement with the DMS profiles. In particular, the early

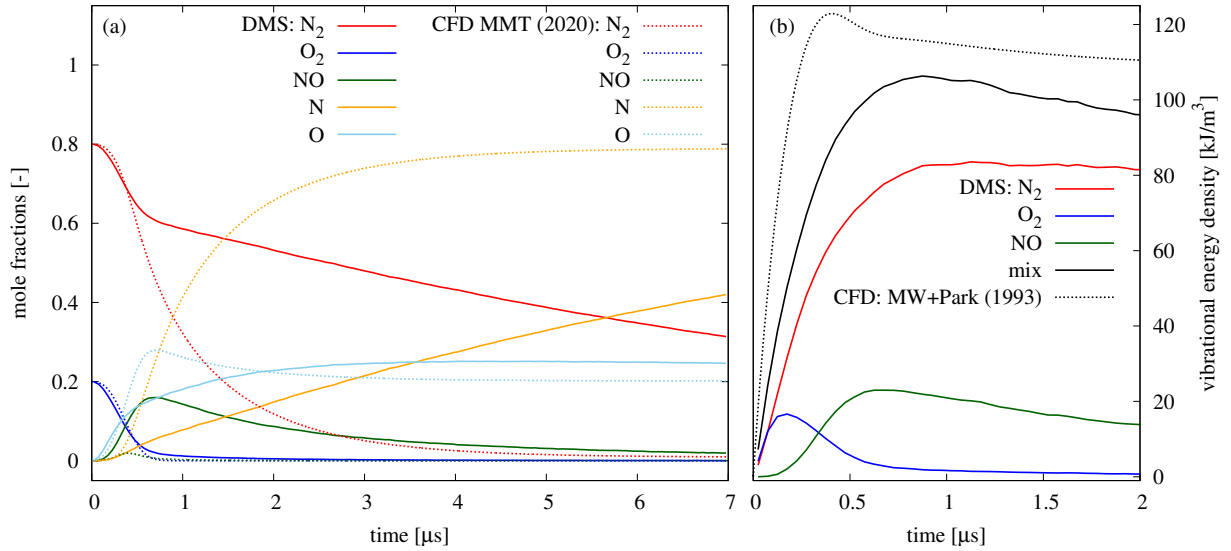

Figure 9: Isothermal heat bath at $T = 10\,000\,\mathrm{K}$. Left: Species mole fractions from DMS (solid lines) vs. US3D with MMT (2020 version) model (dotted lines). Right: vibrational temperatures from DMS (solid lines) vs. US3D with M&W + Park HT correction (dotted lines) for τ_v.

drops in N_2- and O_2-mole fractions (dotted red and blue lines respectively) match the DMS curves (solid lines) much better than was the case in Fig. 8. This can most likely be attributed to the fact that the MMT 2020 nonequilibrium rate coefficients for N_2- and O_2-dissociation were derived from QCT calculations on the same PESs as the ones used by DMS. Past this early stage, the overall mixture compositions in CFD and DMS evolve at noticeably different rates. As was the case when using the Park rates, the mole fractions of atomic nitrogen and oxygen rise much more quickly in the MMT 2020 CFD solution than with DMS. Even though the CFD solution now takes slightly longer than before to approach its final equilibrium composition (nearly at the end of the plotted time), it is still orders of magnitude faster than the DMS solution. As was observed in the previous case, this CFD solution also predicts barely any production of nitric oxide. Recall from Table 3 that the MMT 2020 model used the same rate data as Park for the two exchange reactions. This could explain why its predicted NO-peak lies at the same low level as for the Park model solution. As can be seen in Fig. 9(b), switching to the MMT 2020 chemistry model has only a minor effect on the observed vibrational energy density profile (dotted black line). This makes sense, since the vibrational relaxation rate is still predicted by means of the same M&W + Park HT correlations.

Finally, we repeat the same test case using the most recent MMT reaction set and rate data summarized in Table 4. The CFD mole fraction profiles are shown in Fig. 10(a) (dotted lines) and compared to DMS (solid lines). Now the agreement between both datasets is much better than in any of the two previous runs. Apart from minor deviations, all 5 species mole fractions in the CFD solution track the corresponding DMS profiles over the entire $7\,\mu$s shown in Fig. 10(a). The early drops in N_2- and O_2- mole fraction are captured, as well as the general trends in the rise of atomic nitrogen and oxygen. Most importantly, the CFD solution now exhibits a clear peak in NO- mole fraction (dotted green line), of similar magnitude and occurring at the same time as in the DMS solution (solid green line). In fact, the NO- mole fraction peak is now slightly higher than in the DMS profile. Overall, the CFD-profiles track the DMS-predictions much more reliably than in the other two cases. This is clearly a consequence of ensuring that the set of reactions in the CFD calculations, along with their corresponding kinetic parameters is the most consistent with DMS. In particular, updating the rate parameters for the two Zel'dovich reactions seems to have had a major effect on the NO-profile observed. Furthermore, excluding reactions from the CFD model currently not present in the DMS solution has further helped bring both predictions closer together.

Smaller discrepancies between both datasets can still be observed at very early times, during the first microsecond. Early on, atomic oxygen and nitrogen now rise more slowly in the CFD solution than in DMS (dotted light blue and orange lines vs. solid ones), while slightly more nitric oxide is produced in the CFD

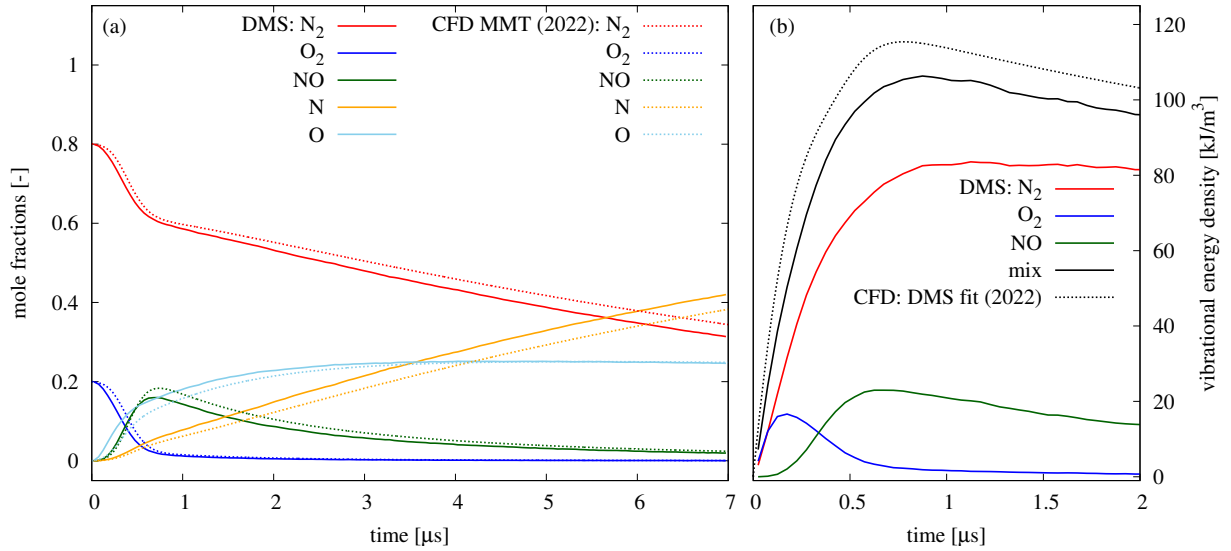

Figure 10: Isothermal heat bath at $T = 10\,000\,\mathrm{K}$. Left: Species mole fractions from DMS (solid lines) vs. US3D with MMT (2022 version) model (dotted lines). Right: vibrational temperatures from DMS (solid lines) vs. US3D with DMS fits (dotted lines) for τ_v.

solution. We suspect that both effects can be explained by a feature of the DMS solution not mentioned so far. Apart from the reaction set listed in Table 4, the DMS calculation simulates a few additional reactions not present in the MMT 2022 list. In particular, trajectories on the N_2O_2 PES can lead to three additional reactions not discussed so far: $N_2 + O_2 \rightleftharpoons NO + N + O$, $N_2 + O_2 \rightleftharpoons 2\,NO$ and $N_2 + O_2 \rightleftharpoons 2\,N + 2\,O$. The existence of these reactions was known to Chaudhry et al. [11], but they were not explicitly included in the original MMT model. Thus, no rate parameters for these reactions are currently available. Furthermore, the DMS calculation accounts for chemical reactions between NO – NO collision pairs (albeit on only 1/12 of all collisions [4]). Such collisions can lead to dissociation of nitric oxide, as well as production of small amounts of N_2- and O_2-molecules through an exchange mechanism. These reactions are also currently not included in the CFD model and their absence there could explain why the NO-mole fraction peaks at a slightly lower value in the DMS solution. In future work, we plan to perform additional QCT on the N_2O_2 PES in order to add these missing reactions to the MMT data set.

The second modification intended to make the CFD solution agree better with DMS concerned the method to estimate vibrational relaxation times. For this last calculation, we switched to using our custom fits for all species pairs relaxation, as discussed in Sec. 3. The result of these changes is reflected in the vibrational energy profiles of Fig. 10(b). As can be seen, the CFD E_v-curve (dotted black line) now tracks the DMS equivalent (solid black line) more closely than in the previous two cases. The agreement is not perfect, with the CFD solution still predicting a slightly higher vibrational energy density overall. The general trends observed with both methods are now in closer agreement than before, though introducing the custom fits for τ_v seems to only have caused a minor improvement. Ultimately, at the conditions of this test case, vibrational relaxation only seems to be of secondary importance and the primary driver for the evolution of the gas state are the chemical reactions. These reactions occur at time scales much larger than the vibrational relaxation. Thus, swapping out chemistry models and rate parameters has a much more significant effect on the solution obtained.

Before concluding this section, we examine the long-term evolution of the gas state for this test case. DMS calculations are computationally costly and were only carried out for the first $7\,\mu$s shown in Figs. 8-10. However, having established that the MMT 2022 model does a fairly good job of reproducing the DMS behavior, we can use CFD to extrapolate the solution much farther in time. We can also examine the effect of recombination reactions on the mixture composition. It should be noted that DMS does not currently model recombination reactions. This does not constitute a major issue, as long as DMS is used to only simulate the early evolution of a shock-heated gas, when recombination reactions are known to have

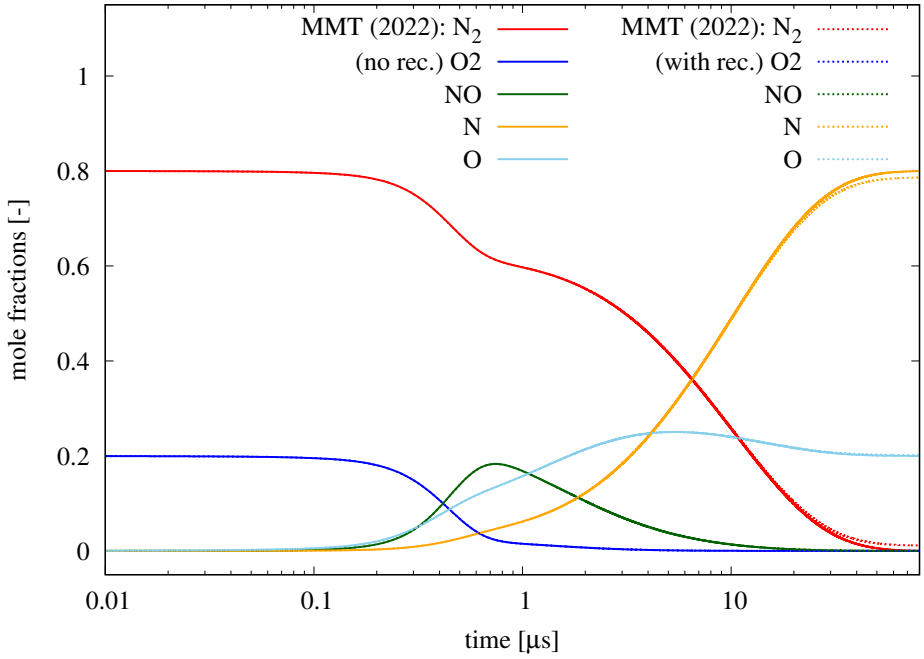

Figure 11: Isothermal heat bath at $T = 10\,000\,\mathrm{K}$. Long-term evolution of US3D solution with MMT (2022 version) model, dissociation only (solid lines) vs. including recombination (dotted lines).

a negligible effect. But as atomic species begin to accumulate in the gas, recombination reactions become increasingly frequent and eventually need to be taken into account. By contrast, dissociation reactions in US3D can easily be modeled as reversible (i.e. including recombination), or "forward-only" (i.e. without recombination) by switching detailed balance relations on or off. Thus, CFD can be used to generate solutions for both cases. The resulting evolution of the mixture compositions is shown in Fig. 11. Since approach to the final equilibrium state takes much longer than the $7\,\mu$s examined previously, a logarithmic time scale is used. The solution without recombination reactions is plotted with solid lines, while the one including recombination uses dotted lines. As would be expected, when recombination reactions are excluded, the gas eventually dissociates completely, with only N and O atoms remaining (solid orange and light blue lines). Since their elemental mole fractions must be conserved, they asymptotically reach the same 80%/20% ratio as was imposed for the initial numbers of nitrogen to oxygen molecules. When recombination is included, the mixture composition follows a slightly different path (dotted lines). At the conditions of this test case, the effect is minor. But approximately past the first $20 - 30\,\mu$s, recombination reactions act to prevent full dissociation of nitrogen. Trace amounts of molecular oxygen and nitric oxide remain, but are too small to be observed at the scale of the plot. The fact that differences between both solutions only appear past the first $20\,\mu$s confirms that excluding them from the DMS calculation did not significantly affect its predictive capability.

5 Conclusions and future work

In this paper, we have presented verification studies for the recently proposed Modified Marrone-Treanor thermochemical nonequilibrium model for computational fluid dynamics. We discussed modifications and enhancements to the thermodynamics, the vibrational relaxation and nonequilibrium chemistry models, which improve its predictive capabilities for flows involving high-temperature air mixtures. We have verified our CFD results by means of Direct Molecular Simulations that rely only on *ab initio* potential energy surfaces to determine all collision outcomes. In particular, we have found that updating the MMT kinetic rate data for the Zel'dovich exchange reactions from the original Park rates to our most recent QCT-derived ones significantly improves the agreement of CFD solutions with DMS. Additional QCT studies are planned,

in order to generate rate data for reactions currently absent from the MMT chemistry mechanism. Further verification of the MMT model against DMS results over a range of temperatures is underway. On-going research also aims to validate the MMT model with recent experimental data [15, 16].

Acknowledgments

We wish to thank Dr. Ioannis Nompelis at the University of Minnesota for his help with integrating our models into US3D.

This work is supported by AFOSR grant FA9550-19-1-0219 and NASA grant 80NSSC20K1061

References

[1] R.S. Chaudhry, I.D. Boyd, E. Torres, T.E. Schwartzentruber, and G.V. Candler. Implementation of a Chemical Kinetics Model for Hypersonic Flows in Air for High-Performance CFD. In *AIAA Scitech 2020 Forum*, 2020. AIAA 2020-2191.

[2] T.E. Schwartzentruber, M.S. Grover, and P. Valentini. Direct Molecular Simulation of Nonequilibrium Dilute Gases. *Journal of Thermophysics and Heat Transfer*, 32(4):892–903, 2018.

[3] G.A. Bird. *Molecular Gas Dynamics and the Direct Simulation of Gas Flows*. Oxford University Press, 1994.

[4] E. Torres, E.C. Geistfeld, and T.E. Schwartzentruber. Direct molecular simulation of rovibrational relaxation and chemical reactions in air mixtures. In *AIAA SCITECH 2022 Forum*, 2022.

[5] R.J. Duchovic, Y.L. Volobuev, G.C. Lynch, A.W. Jasper, D.G. Truhlar, T.C. Allison, A.F. Wagner, B.C. Garrett, J. Espinosa García, and J.C. Corchado. POTLIB library. http://comp.chem.umn.edu/potlib.

[6] G.V. Candler, H.B. Johnson, I. Nompelis, P.K. Subbareddy, T.W. Drayna, and V. Gidzak. Development of the US3D Code for Advanced Compressible and Reacting Flow Simulations. In *53rd AIAA Aerospace Sciences Meeting, Kissimmee, Florida*, 2015. AIAA 2015-1893.

[7] E. Torres and T.E. Schwartzentruber. Direct molecular simulation of oxygen dissociation across normal shocks. *Theoretical and Computational Fluid Dynamics*, 36(1):41–80, 2022.

[8] C Park. Review of Chemical-Kinetic Problems of Future NASA Missions, I: Earth Entries. *Journal of Thermophysics and Heat Transfer*, 7(3):385–398, 1993.

[9] R.C. Millikan and D.R. White. Systematics of Vibrational Relaxation. *Journal of Chemical Physics*, 39(12):3209–3214, 1963.

[10] J.D. Bender, P. Valentini, I. Nompelis, Y. Paukku, Z. Varga, D.G. Truhlar, T.E. Schwartzentruber, and G.V. Candler. An improved potential energy surface and multi-temperature quasiclassical trajectory calculations of $N_2 + N_2$ dissociation reactions. *The Journal of Chemical Physics*, 143:054304, 2015.

[11] R.S. Chaudhry, J.D. Bender, T.E. Schwartzentruber, and G.V. Candler. Quasiclassical Trajectory Analysis of Nitrogen for High-Temperature Chemical Kinetics. *Journal of Thermophysics and Heat Transfer*, 32(4):833–845, 2018.

[12] R.S. Chaudhry, I.D. Boyd, and G.V. Candler. Vehicle-Scale Simulations of Hypersonic Flows using the MMT Chemical Kinetics Model. In *AIAA Aviation 2020 Forum*, 2020. AIAA 2020-3272.

[13] M.E. Holloway, R.S. Chaudhry, and I.D. Boyd. Assessment of hypersonic double-cone experiments for validation of thermochemistry models. *Journal of Spacecraft and Rockets*, 59(2):389–400, 2022.

[14] P. Sawicki, R.S. Chaudhry, and I.D. Boyd. Influence of chemical kinetics models on plasma generation in hypersonic flight. *AIAA Journal*, 60(1):31–40, 2022.

[15] J.W. Streicher, A. Krish, R.K. Hanson, K.M. Hanquist, R.S. Chaudhry, and I.D. Boyd. Shock-tube measurements of coupled vibration–dissociation time-histories and rate parameters in oxygen and argon mixtures from 5000 k to 10 000 k. *Physics of Fluids*, 32(7):076103, 2020.

[16] J.W. Streicher, A. Krish, and R.K. Hanson. Vibrational relaxation time measurements in shock-heated oxygen and air from 2000 k to 9000 k using ultraviolet laser absorption. *Physics of Fluids*, 32(8):086101, 2020.